

# Intelligent Power Compensation System Based on Adaptive Sliding Mode Control Using Soft Computing and Automation

Qidan Zhu<sup>a</sup>, Zhibo Yang<sup>a\*</sup>

<sup>a</sup> College of Automation, Harbin Engineering University, Harbin 150001, China

The approach power compensator system (APCS) plays a role in the automatic carrier landing system (ACLS), and the performance of the APCS is affected by the carrier air-wake in the final-approach. In this paper, the importance of the APCS is verified through the analysis of the signal flow chart of the ACLS. Hence, it is necessary to suppress the carrier air-wake in order to improve the anti-interference ability. The adaptive sliding mode control (ASMC) not only has better dynamic tracking performance compared to the nonlinear mode, but also can efficiently resist the disturbance caused by the carrier air-wake. The design of the longitudinal control law of the ACLS is based on the carrier-based aircraft nonlinear model and the carrier air-wake model. It comprises the longitudinal guidance rate, autopilot (CAS) and the APCS. The ASMC is used to design the APCS to suppress the carrier air-wake. A comparison of the simulation results indicates that the design based on the ASMC has better anti-interference ability and can keep the velocity constant on the timely.

Keywords: automatic dynamic compensation system; speed stability; the carrier air-wake; the adaptive sliding mode control

## 1. INTRODUCTION

The APCS plays an important role in the carried landing task of the aircraft. In the final-approach, the velocity of the carrier-based aircraft will decrease at the back as shown in Figure. 1. As a result, the drag will increase along with the decreasing speed. Therefore, the drive force of the aircraft must be compensated for in order to keep the balance of the force to maintain the flight-path within a safe range. There are two ways to design the APCS: by keeping the velocity constant or keeping the angle of attack (AOA) constant. [1] Because the ship burble of the carrier air-wake will be disturbed and is not conducive to the carrier landing, the APCS should also be designed to suppress burble generated by the carrier air-wake.[2]

[3–5] used the complex domain method to prove the necessity

of the APCS in the rear of the aircraft. However, the complex domain analysis is an abstract and general method, and does not consider the system's components and physical process of the analysis object.

In the practical application of the two designs (keeping the velocity constant or keeping the angle of attack (AOA) constant), it is necessary to compare differences in performance. The two designs must be compared to identify which method can yield good performance. [6] proved that keeping the AOA constant automatically adjusts the thrust of the engine and has strong anti-interference ability. In the '50s of the last century, the US Navy thought that keeping the AOA constant is better than keeping the velocity constant in the automatic carrier landing. [7]

Several researches have thoroughly investigated the speed stability of the APCS to explain the reasons for the unstable speed. The carrier-based aircraft is affected by the ship burble of the carrier air-wake in the final-approach and has

\*Correspondence Author: Email: yzblsn@163.com

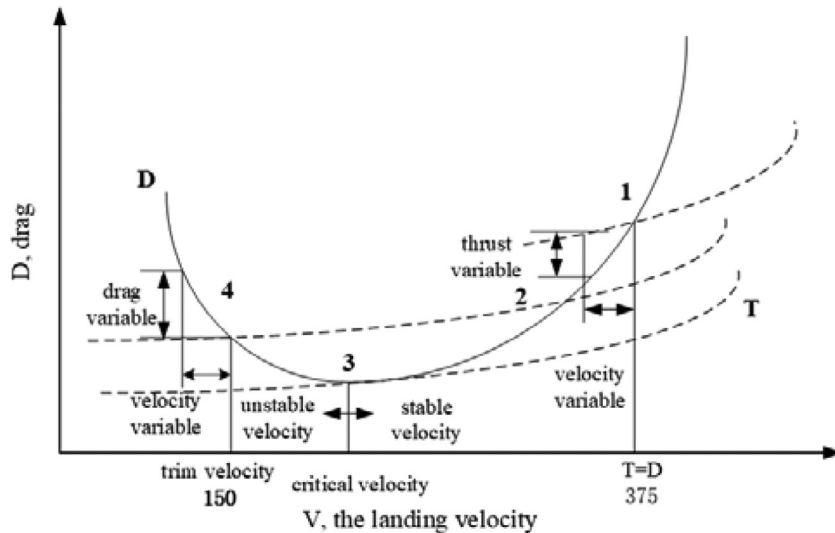


Figure 1 Curves of drag and thrust.

a strong coupling and nonlinear dynamics characteristic. [8] It is necessary to use nonlinear control in the design of the APCS to suppress the carrier air-wake. Nonlinear dynamic inversion and global sliding mode variable structure control technology is applied to a class of uncertain nonlinear systems, and this control strategy is applied to the attitude tracking problem of spacecraft. [9] [10] designed the discrete-time variable structure APCS with disturbance compensation to suppress burble, but it used the linear model which cannot accurately express the dynamic performance of aircraft. The adaptive fuzzy control strategy is used to solve the problem of rudder failure and wind disturbance during landing. [11] [12] designed the APCS based on a high-order sliding mode to keep the AOA constant; it ensures that the flight path of the carrier-based aircraft can respond to the pitch attitude command accurately and quickly in the final-approach. [13] uses the theory of the LMI (linear matrix inequality) to design the APCS; it ensures that the carrier-based aircraft can maintain excellent flight attitude, and suppresses the disturbance of the carrier air-wake.

Through the theoretical analysis of the relationship between resistance and velocity, the velocity stability criterion is obtained, which proves that the velocity stability of the carrier-based aircraft is unstable in the final-approach. In the above studies, [9], [11] and [12] do not consider the estimation and compensation of the carrier air-wake. [10] and [13] use the linear method, although this method may be invalid due to the nonlinear and strong coupling of the carrier-based aircraft in the final-approach. Therefore, because of the nonlinear and strong coupling of the carrier-based aircraft, the nonlinear dynamic model is applied. The design of the APCS based on the ASMC takes into account the practicability of sliding mode control method in aircraft control design, and is combined with adaptive control theory which can estimate and compensate for the disturbance of the carrier air-wake. is designed. Meanwhile, the introduction of a hyperbolic tangent function reduces the chattering of the system caused by sliding mode control. The APCS system designed in this paper can effectively suppress the deviation of the angle of attack and reduce the chattering.

## 2. THE ACLS MODEL

### 2.1 The Nonlinear Model of the Carrier-Based Aircraft in the Final-Approach

The state changes of the carrier landing are shown in Fig. 2, The ACLS has begun to work in the final-approach, which includes the APCS. The following assumptions are made when analyzing the force of the carrier-based aircraft in flight. [14–16]

1. The aircraft are fixed relative to each other. This assumption is valid for the carrier-based aircraft.
2. The geometric structure of the airframe is symmetrical along the longitudinal plane of the airframe. It can be seen that the sum of the two inertia products of the airplane is zero. This assumption is also valid for the carrier-based aircraft.
3. When the flight altitude is less than 40 km and the speed is less than 3 Mach, the influence of the Earth's curvature and rotation on the flight performance is very small, so the gravity field model which is a plane parallel model can be used to establish the inertial system. It is noteworthy that this assumption is feasible for aircraft control design, but not applicable to the analysis of the inertial navigation system.
4. It is necessary to assume that the mass of an aircraft remains unchanged, ignoring factors such as fuel consumption when applying Newton's law of motion.

A large number of simulations show that the influence of atmospheric disturbance on carrier-based aircraft is mainly due to the vertical trajectory error caused by the vertical disturbance components. In view of this, the focus of this paper is only on the longitudinal flight path control of carrier-based aircraft, and we establish a standard longitudinal nonlinear mathematical model for a certain type of carrier-based aircraft. [17]

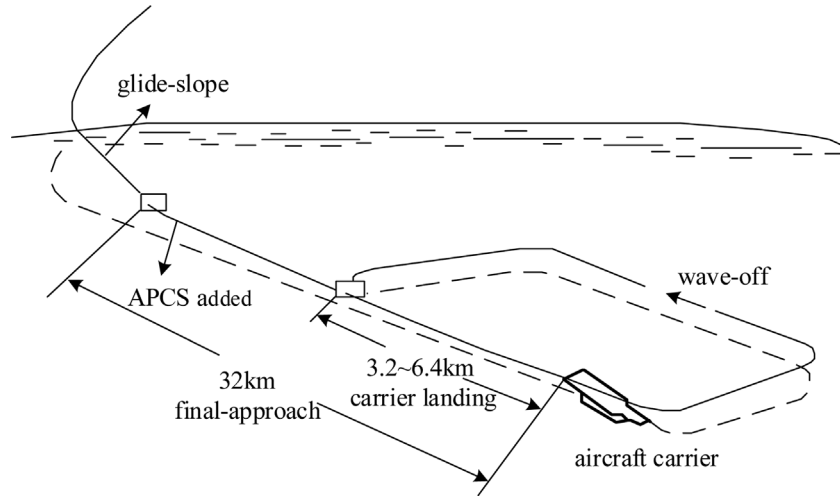


Figure 2 Schematic Diagram of APCS added to ACLS.

$$P = \frac{mV}{\sin \alpha} \left[ -\frac{1}{mV}L + q - \dot{\alpha} + \frac{g}{V}(\cos \theta \cos \alpha + \sin \alpha \sin \theta) \right] \quad (1)$$

$$\dot{V} = \frac{P \cos(\alpha) - D}{m} - g \sin \gamma \quad (2)$$

$$\dot{\gamma} = \frac{L + P \sin(\alpha)}{mV} - \frac{g}{V} \cos(\gamma) \quad (3)$$

$$\dot{H} = V \sin \gamma \quad (4)$$

$$\dot{q} = \frac{M}{I_y} \quad (5)$$

where the scalar total engine thrust of the carrier-based aircraft is  $P$ ; the angle of attack is  $\alpha$ ; the flight-path angle is  $\gamma$ ; the pitch attitude is  $\theta$ ; the inertial velocity is  $V$ ; the  $H$  is the altitude; the  $C_D$  is the drag coefficient;  $\delta_e$  is the elevator deflection angle;  $\delta_c$  is the canard deflection angle;  $C_L$  is the lift coefficient,  $C_M$  is the pitch torque coefficient;  $q$  is the pitch rate;  $\rho$  is the air density,  $S$  is the reference area of the wing,  $M$  is the pitch torque, and  $I_y$  is the moment of pitch inertia.

## 2.2 The Model of the Carrier Air-Wake

In this paper, the engineering model of the air-wake is described as the MIL-HDBK-1797, which has good practical application and is widely used. The model regards the air-wake disturbance as the sum of four components, and describes them quantitatively. It is also stipulated that the model can be used to test the landing performance of carrier aircraft in the final-approach. The simulation expression of each velocity component is described in detail in the MIL-HDBK-1797.

$$\begin{cases} u = u_1 + u_2 + u_3 + u_4 \\ v = v_1 + v_4 \\ w = w_1 + w_2 + w_3 + w_4 \end{cases} \quad (6)$$

The velocity of the carrier air-wake can be decomposed into longitudinal component  $u$ , transverse component  $v$  and vertical component  $w$ . The  $u$  is parallel to the direction of deck wind which select forward is positive, the  $v$  is positive along the direction of the pilot's right hand which select down is positive.

According to the manual, the carrier air-wake consists of random free-air turbulence, steady ship-wake disturbance, periodic ship-motion-induced turbulence and random ship-wake disturbance. the random free-air turbulence consists of  $u_1$ ,  $v_1$ , and  $w_1$ . The steady ship-wake disturbance consists of  $u_2$  and  $w_2$ . The periodic ship-motion-induced turbulence consists of  $u_3$  and  $w_3$ , and the random ship-wake disturbance consists of  $u_4$ ,  $v_4$  and  $w_4$ . The formula can be used to calculate the complete velocity of the ship burble.

When the flight speed is 70 m/s, the deck wind is 15 m/s, and the track angle is  $-3.5$  degrees, the air-wake simulation results can be obtained as follows.

## 3. THE ANALYSIS OF THE SPEED STABILITY

The signal flow chart of the carrier-based aircraft is shown in Figure 4. The lift, drag and pitch torque of carrier-based aircraft in the final-approach can be expressed as Eq. (6–8). Through the analysis of velocity signal feedback, it can be concluded that the effect of drag on velocity is either direct or indirect. The direct effect is that velocity changes directly produce drag components to drag force. The indirect effect is that speed variation produces the variables of pitch attitude and fight path angle through pitch torque loop and lift force loop. The variation of AOA can be determined by Eq. (9), and the variation of AOA affects the drag component of the drag loop. The variation of drag affects the velocity change through feedback channels which are affected by the APCS.

$$D = \frac{1}{2} \rho V^2 S C_D(\alpha, \delta_e, \delta_c) \quad (7)$$

$$L = \frac{1}{2} \rho V^2 S C_L(\alpha, \delta_e, \delta_c) \quad (8)$$

$$M = \frac{1}{2} \rho V^2 S \bar{c} C_M(\alpha, q, \delta_e, \delta_c) \quad (9)$$

$$Q = \alpha + \gamma \quad (10)$$

Draw the velocity change relation of carrier-based aircraft as shown in Figure 5. Besides, the relationship between AOA,

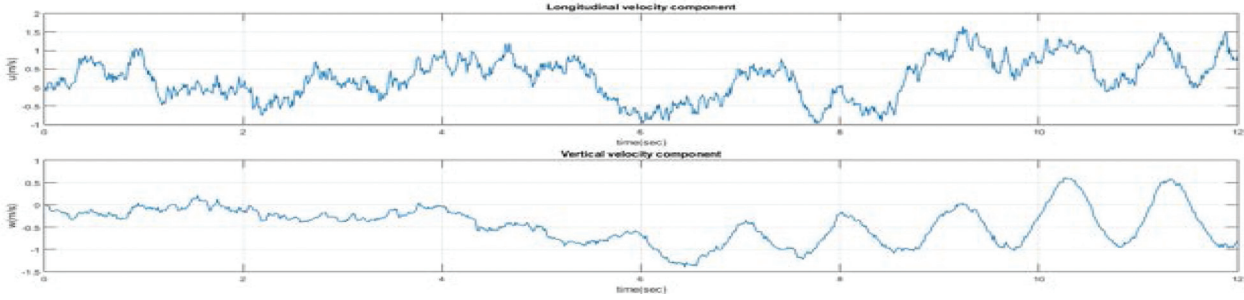


Figure 3 Complete time history simulation results to the carrier air-wake.

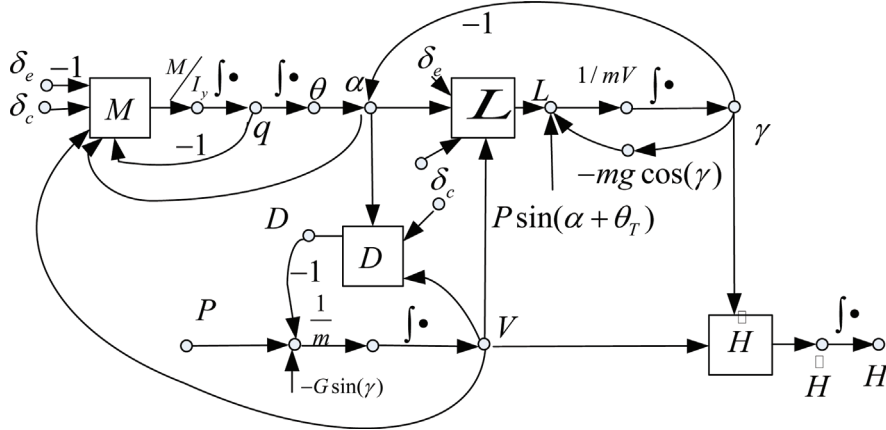


Figure 4 The signal flow chart of the ACLS.

flight path angle and pitch attitude is discussed. It is known that the dynamic characteristics of the flight path angle and pitch attitude are very important for the carrier-based aircraft in the final-approach. At the same time, the APCS can ensure the good tracking ability of the glide slope; hence, carrier-based aircraft need the APCS in the final-approach.

The loop of the velocity is of great help in judging the stability of speed. Through the velocity change relation of carrier-based aircraft, when the velocity signal is transmitted to the pitch torque loop and the lift loop, the two loops will feed back to the velocity. It is assumed that when the velocity of the carrier-based aircraft is stable, the pitch torque loop and the lift loop are in equilibrium.

The derivative of the lift loop is shown in Eq. (10).

$$dL = \frac{\partial L}{\partial \alpha_L} d\alpha_L + \frac{\partial L}{\partial V_L} dV_L = 0 \quad (11)$$

The derivative of the pitch torque is shown in Eq. (11).

$$dM = \frac{\partial M}{\partial \alpha_M} d\alpha_M + \frac{\partial M}{\partial V_M} dV_M = 0 \quad (12)$$

The derivative of the AOA is divided into lift and pitch torque which is shown in Eq. (12).

$$\begin{aligned} d\alpha &= d\alpha_L + d\alpha_M \\ &= -dV \left( \frac{\partial L}{\partial V_L} / \frac{\partial L}{\partial \alpha_L} \right) - dV \left( \frac{\partial M}{\partial V_M} / \frac{\partial M}{\partial \alpha_M} \right) \end{aligned} \quad (13)$$

The partial derivative of the lift to velocity and AOA is shown in Eq. (13), and the partial derivative of the pitch torque to velocity and AOA is shown in Eq. (14)

$$\frac{\partial L}{\partial V_L} = \rho V S C_L, \quad \frac{\partial L}{\partial \alpha_L} = 0.5 \rho V^2 S C_{L\alpha} \quad (14)$$

$$\frac{\partial M}{\partial V_M} = \rho V S C_M, \quad \frac{\partial M}{\partial \alpha_M} = 0.5 \rho V^2 S C_{M\alpha} \quad (15)$$

Then, the partial derivative of the drag to the velocity and AOA is shown in Eq. (15).

$$\begin{aligned} \frac{\partial D}{\partial V} &= \rho V S C_D \\ \frac{\partial D}{\partial \alpha} &= 0.5 \rho V^2 S C_{D\alpha} \end{aligned} \quad (16)$$

The  $C_{L\alpha}$ ,  $C_{D\alpha}$  and  $C_{M\alpha}$  are expressed in Eq.(16).

$$C_{L\alpha} = \frac{\partial C_L}{\partial \alpha}, \quad C_{D\alpha} = \frac{\partial C_D}{\partial \alpha}, \quad C_{M\alpha} = \frac{\partial C_M}{\partial \alpha} \quad (17)$$

The formula (15) can be expressed by Eq. (17)

$$\begin{aligned} \frac{dD}{dV} &= \frac{\partial D}{\partial V} + \frac{\partial D}{\partial \alpha} \frac{\partial \alpha}{\partial V} \\ &= \rho V S [C_D - C_{D\alpha} (C_L/C_{L\alpha} + C_M/C_{M\alpha})] \end{aligned} \quad (18)$$

The  $K_v$  can be obtained as shown in Eq. (18)

$$\begin{aligned} K_V &= -\frac{1}{m} \frac{dD}{dV} = -\frac{1}{m} \rho V S [C_D \\ &\quad - C_{D\alpha} (C_L/C_{L\alpha} + C_M/C_{M\alpha})] \end{aligned} \quad (19)$$

When the  $K_v$  is greater than zero, the speed is in a stable state, and Eq. (19) can be obtained at this time. However, when  $K_v$  is less than zero, the speed is in an unstable state.

$$\frac{C_D}{C_{D\alpha}} < \frac{C_L}{C_{L\alpha}} + \frac{C_M}{C_{M\alpha}} \quad (20)$$

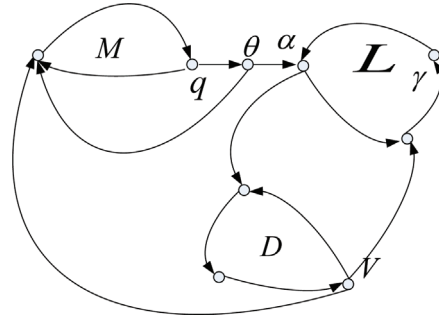


Figure 5 The velocity change relation of carrier-based aircraft.

Eq. (19) can be regarded as the criterion for speed stability. The speed stability changes in the final-approach of the carrier-based aircraft can be judged accurately according to the criterion, and it can be deduced that the speed stability is related to the derivative value of lift, resistance and pitching moment.

In this work, we build a nonlinear model; the aerodynamic coefficient and derivative of aerodynamic are shown in Table 1. It has been proved that the speed is unstable during the carrier landing task when the aerodynamic parameters and derivative are brought to the Eq. (19). It can be concluded that the carrier-based aircraft needs the APCS in order to maintain speed stability.

## 4. THE NORMAL DESIGN OF THE APCS

### 4.1 The Normal Design of the APCS

Referring to the ACLS design of the F/A-18 aircraft, the longitudinal ACLS design of carrier-based aircraft is carried out based on H-dot command mode, which mainly includes a control augmentation system (CAS), an approach power compensation system (APCS) and a longitudinal guidance law. For the longitudinal guidance rate and the autopilot design, refer to [18].

The main task of the APCS is to enable the carrier-based aircraft to automatically adjust the throttle of the engine during carrier landing, thereby supplementing thrust to maintain the velocity and angle of attack of the aircraft, and to achieve the accurate tracking of the command path of the carrier-based aircraft. The structure diagram of the APCS was shown in Figure 7, and the structure of the control law can be obtained by Eq. (20) [18].

$$\Delta\delta_{pl} = K_e\Delta\delta_e + \left(K_{\alpha P} + K_{\alpha I}\frac{1}{S}\right)\Delta\alpha + K_q\Delta q + K_{n_z}\Delta n_z \quad (21)$$

The formula shows that the APCS can ensure that the carrier-based aircraft flight is more stable and the deviation of the AOA can be rectified so that the carrier-based aircraft can land smoothly along the ideal glide slope.

### 4.2 The ASMC Design of the APCS

The carrier air-wake will cause disturbance of the AOA in the final-approach, which is not conducive in carrier landing task. Therefore, the APCS is designed to suppress the disturbance generated by the air-wake and ensure that the AOA remains

constant in the final-approach. Due to the PID controller which is applied in the conventional design of APCS, the latter's ability to suppress the disturbance is poor. Hence, the new APCS based is designed by the adaptive sliding mode control strategy.

Through the nonlinear model of the carrier-based aircraft, the relationship between thrust and AOA can be obtained by Eq. (21).

$$P = \frac{mV}{\sin\alpha} \left[ \frac{-\frac{1}{mV}L + q + \frac{g}{V}\cos}{(\cos\theta\cos\alpha + \sin\alpha\sin\theta) - \dot{\alpha}} \right] \quad (22)$$

Formula (21) can be converted to formula (22).

$$\dot{\alpha} = -\frac{1}{mV}L + \frac{g}{V}(\cos\theta\cos\alpha + \sin\alpha\sin\theta) - \frac{P\sin\alpha}{mV} \quad (23)$$

In order to simplify Eq. (22), the following assumptions are obtained by Eq. (23) and Eq. (24).

$$f_1(\alpha) = -\frac{1}{mV}L + \frac{g}{V}(\cos\theta\cos\alpha + \sin\alpha\sin\theta) \quad (24)$$

$$f_2(\alpha) = -\frac{\sin\alpha}{mV} \quad (25)$$

Then Eq. (22) can be simplified as Eq. (25).

$$\dot{\alpha} = f_1(\alpha) + f_2(\alpha)2u + \lambda \quad (26)$$

where the  $\lambda$  is the system interference source. The tracking error can be defined by Eq.(26)

$$e = \alpha - \alpha_d \quad (27)$$

Then, the sliding surface can be selected with Eq.(27) where the  $k_1$  is constant.

$$s = e + k_1 \int e \quad (28)$$

The derivative of the sliding mode function can be obtained with Eq.(28).

$$\begin{aligned} \dot{s} &= \dot{\alpha} - \Delta\dot{\alpha} + k_1e \\ &= f_1(\alpha)_2 + f_2(\alpha)_2u + \lambda - \Delta\dot{\alpha} + k_1e \end{aligned} \quad (29)$$

The control input of the system can be obtained with Eq.(31).

$$u = \frac{1}{f_2} \left( \Delta\dot{\alpha} - f - k_1e - \hat{\lambda} \operatorname{sgn}(s) - k_s s \right) \quad (30)$$

Because the  $\operatorname{sign}(s)$  in Eq. (29) can cause the dithering of the state of the system on the sliding surface, this will affect the accuracy of control and increase the energy consumption of the

**Table 1** The values of aerodynamic coefficients and dynamic coefficient derivatives.

Coefficient	$C_L$	$C_L$	$C_M$	$C_{D\alpha}$	$C_{L\alpha}$
Value	1.1121	0.2213	$1.132 \times 10^{-6}$	0.0608	0.015
Coefficient	$C_{M\alpha}$	$C_D/C_{D\alpha}$	$C_L/C_{L\alpha}$	$C_M/C_{M\alpha}$	
Value	0.0178	18.2886	14.7395	3.3613	

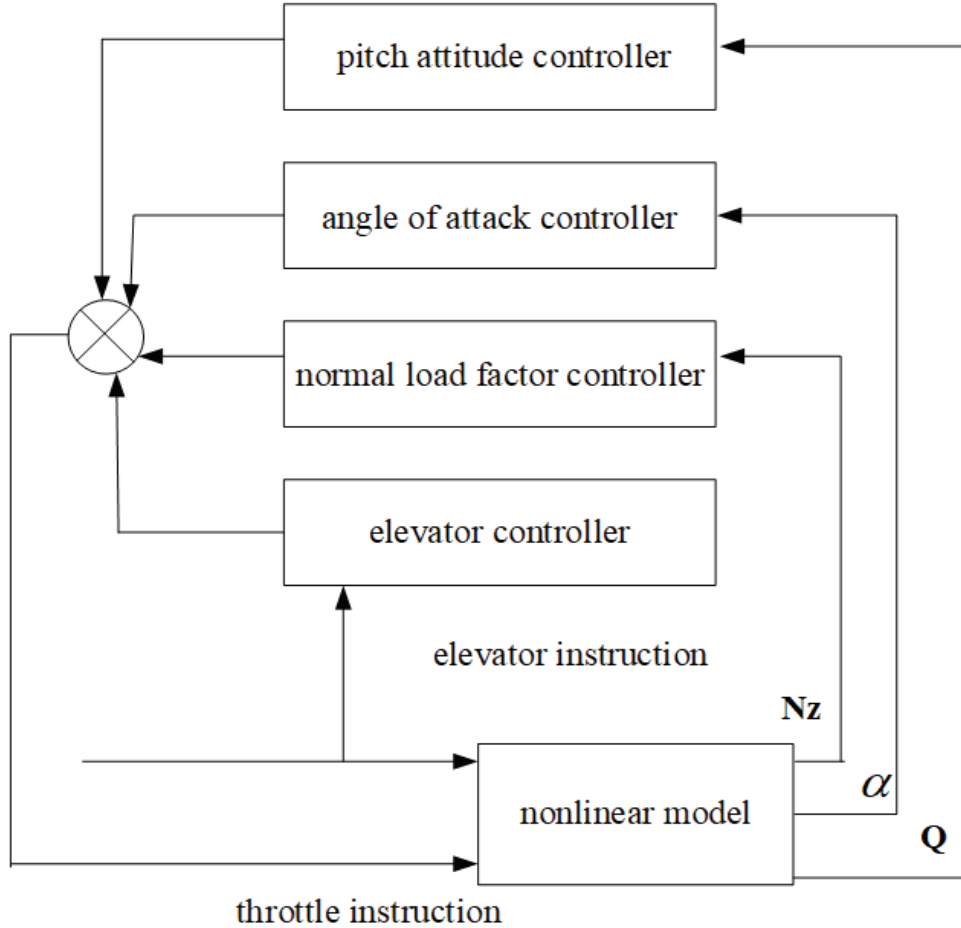


**Figure 6** Diagram of the APCS structure.

system as explained in [19]. In order to reduce dithering, the hyperbolic tangent function is used instead of the sign function as in Eq. (30).

$$\tanh(k_2z) = \frac{e^{k_2z} - e^{-k_2z}}{e^{k_2z} + e^{-k_2z}} \quad (31)$$

where the  $z$  is the independent variable of the function,  $k$  is the control parameter of slope. The boundary value at both ends of the hyperbolic tangent function is the same as the symbolic function. But near the origin, the hyperbolic tangent function makes the value of the function change smoothly which has a certain slope, there is no smooth change near the origin of the symbolic function. Let  $\Delta$  be the minimum positive value of the hyperbolic tangent function when it is equal to 1. The area between  $\Delta$  and  $-\Delta$  is a “boundary layer”. When the hyperbolic tangent function is used, the controller uses switch control outside the boundary layer. But in the boundary layer, the controller adopts the approximate linear feedback control, and the two modes can switch smoothly. This is why the hyperbolic tangent function can reduce chattering.

The Lyapunov function is selected as Eq. (31).

$$V = \frac{1}{2}s^2 + \frac{1}{2\gamma}\hat{\lambda}^2 \quad (32)$$

The derivative of the Lyapunov function can be expressed as Eq. (32).

$$\begin{aligned} \dot{V} &= s\dot{s} + \frac{1}{\gamma}\tilde{\lambda}\dot{\lambda} \\ &= s(f_1 + f_2u + \lambda - \Delta\ddot{\alpha} + k_1e) + \frac{1}{\gamma}(\lambda - \hat{\lambda})(\dot{\lambda} - \dot{\hat{\lambda}}) \end{aligned} \quad (33)$$

Eq. (31) can be taken into Eq. (32), then Eq. (33) can be obtained.

$$\begin{aligned} \dot{V} &= s(f_1 - f_1 - \hat{\lambda} \tanh(ks) - k_1e - k_s s \\ &\quad + \Delta\ddot{\alpha} + \lambda - \Delta\ddot{\alpha} + k_1e) + \frac{1}{\gamma}(\lambda - \hat{\lambda})\dot{\lambda} \end{aligned}$$

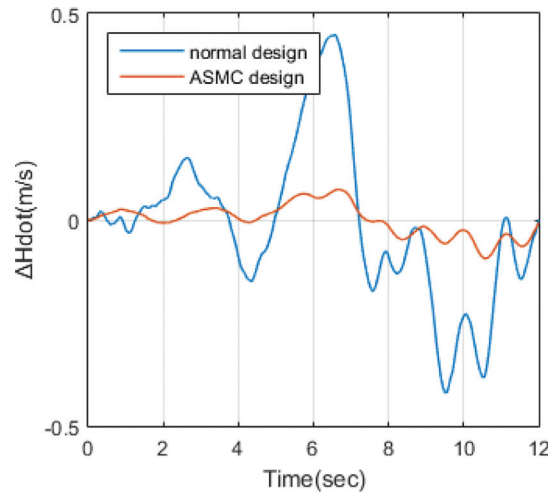


Figure 7 Comparison of the vertical rate in carrier air-wake.

$$\begin{aligned}
 &= s \left( -k_s s - \hat{\lambda} \tanh(ks) + \lambda \right) + \frac{1}{\gamma} (\lambda - \hat{\lambda}) \dot{\lambda} \\
 &= -k_s s^2 + (\lambda - \hat{\lambda} \tanh(ks))s + \frac{1}{\gamma} (\lambda - \hat{\lambda}) \dot{\lambda} \quad (34)
 \end{aligned}$$

In order to better estimate and compensate for the air-wake disturbance, the adaptive law can be selected as Eq. (34) [20].

$$\dot{\hat{\lambda}} = -\gamma s \quad (35)$$

Finally, Eq. (35) can be obtained.

$$\begin{aligned}
 \dot{V} &= -k_s s^2 + (\lambda - \hat{\lambda} \tanh(ks))s - \frac{1}{\gamma} (\lambda - \hat{\lambda}) \gamma s \\
 &= -k_s s^2 + (\lambda - \hat{\lambda} \tanh(ks))s - (\lambda - \hat{\lambda})s \\
 &= -k_s s^2 + (\hat{\lambda} - \hat{\lambda} \tanh(ks))s
 \end{aligned}$$

$$= \begin{cases} -k_s s^2 + (\hat{\delta} - \hat{\delta})s = -k_s s^2 \leq 0 & s > \Delta \\ -k_s s^2 + (\hat{\delta} - \hat{\delta} \tanh(ks))s \leq -k_s s^2 \leq 0 & |s| \leq \Delta \\ -k_s s^2 + (\hat{\delta} + \hat{\delta})s \leq -k_s s^2 \leq 0 & s < -\Delta \end{cases} \quad \begin{matrix} \tanh(ks) < 1 \\ \tanh(ks) < 1 \end{matrix} \quad (36)$$

The rationality of the existence of the sliding surface is verified and the stability of the system is ensured.

## 5. THEORIES AND SIMULATION ANALYSIS

The carrier air-wake model is added to the ACLS in the final-approach. The simulation results of the unit step response to the carrier air-wake are shown in Figures 8–16 where  $\Delta N_z$  is the normal load factor deviation;  $\Delta H\dot{}$  is the vertical rate deviation;  $\Delta H$  is the altitude deviation;  $\Delta \gamma$  is the flight path angle deviation;  $\Delta \alpha$  is the AOA deviation,  $\Delta Q$  is the pitch attitude deviation;  $\Delta q$  is the pitch rate deviation, and  $\Delta V$  is the velocity deviation.

It can be seen from Figure 7 that the vertical rate deviation creates a slight variation by the burble, and the maximum decreases

from 0.45 m/s to 0.07 m/s. It can be seen from Figure 8 that the maximum altitude deviation decreases from 0.67 m to 0.16 m. Simulation results show that the APCS based on ASMC can assist the carrier-based aircraft to land along the ideal glide slope.

The angle of flight path deviation changes near  $-3.5^\circ$ , as shown in Figure 9. Affected by the burble, the maximum amplitude of the flight path deviation decreases from  $0.39^\circ$  to  $0.06^\circ$ . Simulation results show that the ASMC APCS proposed in this paper achieves the precise control of the flight path angle. It also avoids the large impact load due to the large track angle, and prevents the increasing difficulty, faced by the pilot, of maintaining an accurate glide slope during the carrier's landing due to the small track angle.

The angle of AOA deviation changes near  $8.1^\circ$ , as shown in Figure 10. Affected by the burble, the curve of an AOA deviation fluctuates greatly in a normal design. The maximum amplitude of the AOA deviation is reduced from  $1.68^\circ$  to  $0.34^\circ$ , and the range of variation is far less than that of the US Navy. The simulation results show that the APCS based on ASMC keeps the AOA constant during the carrier landing task by automatically adjusting the thrust of the engine, and the anti-interference ability is obviously improved.

The velocity deviation changes near 70 m/s. The velocity curve is shown in Figure 11, where it can be seen that the maximum amplitude of the velocity deviation decreases from 0.5539 m/s to 0.1011 m/s. The simulation result shows that the APCS based on ASMC maintains a constant velocity to suppress the carrier air-wake better than does the normal design.

Figures 12–13 show that the pitch attitude deviation changes near  $4.6^\circ$ . The decrease of the maximum amplitude is very obvious and the decrease range is reduced from  $1.45^\circ$  to  $0.31^\circ$ , and at the same time, the pitch rate deviation is reduced from  $1.08^\circ$  to  $0.18^\circ$ . Simulation results show that the tracking and robustness of the ASMC APCS designed in this work is better than that of normal design.

The thrust curve is shown in Figure 14. It can be seen that the chattering phenomenon does not appear due to the use of the ASMC. Simulation results show that the sliding mode can be improved and the chattering phenomenon is reduced by the ASMC design presented in this paper.

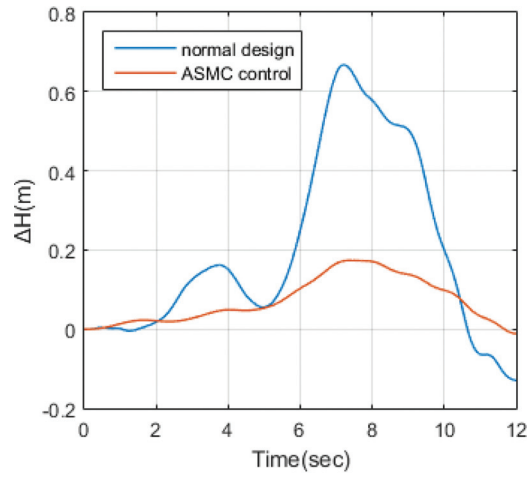


Figure 8 Comparison of the altitude in carrier air-wake.

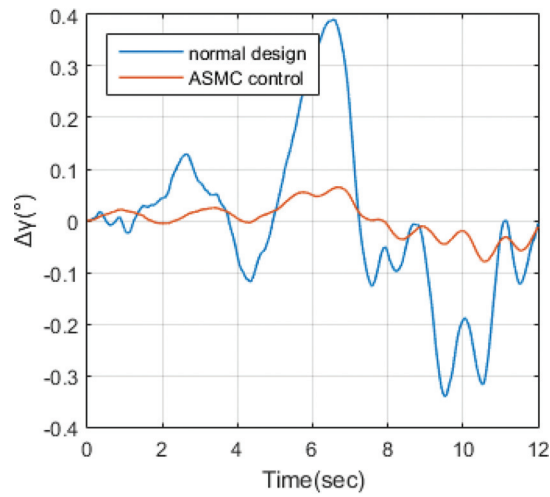


Figure 9 Comparison of the flight path angle in carrier air-wake.

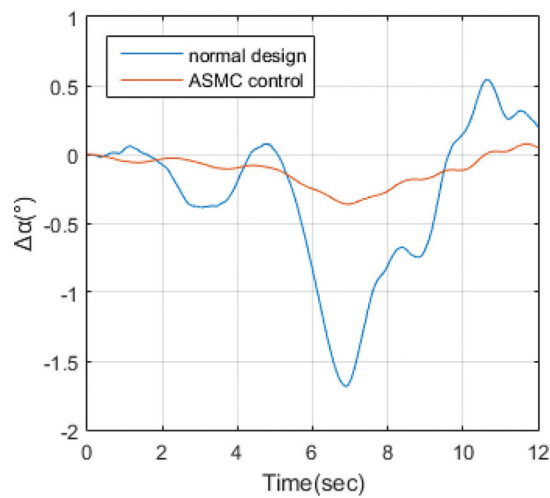


Figure 10 Comparison of the AOA in carrier air-wake.

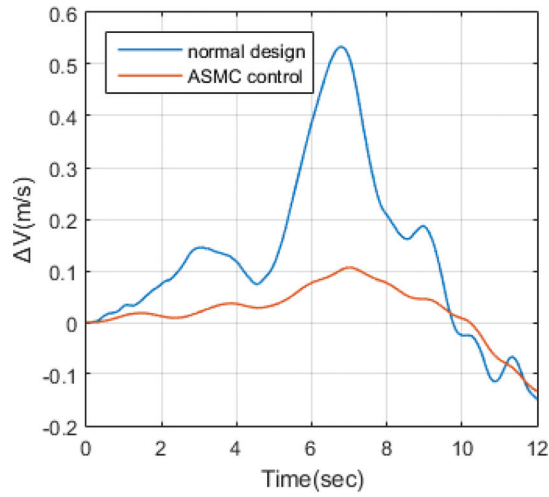


Figure 11 Comparison of the velocity in carrier air-wake.

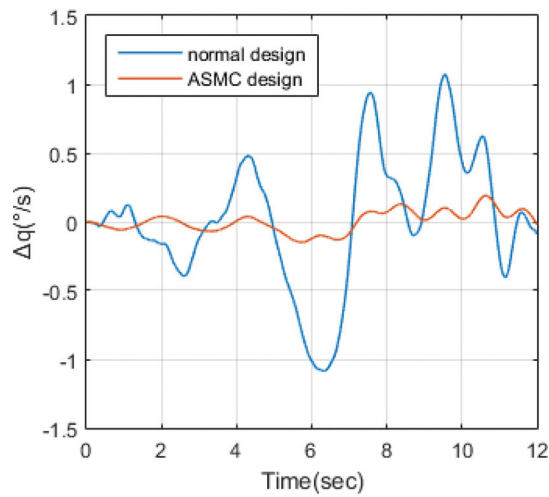


Figure 12 Comparison of the pitch rate in carrier air-wake.

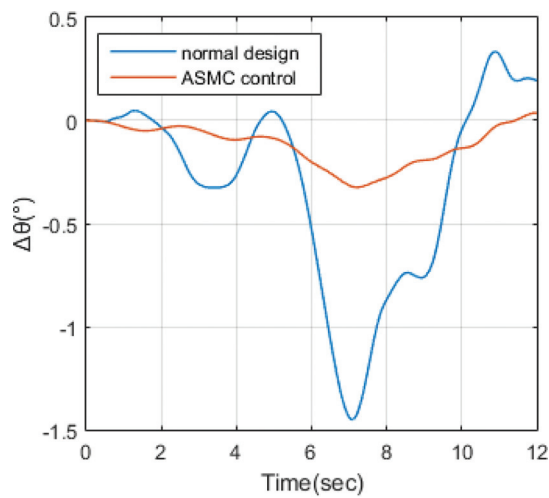


Figure 13 Comparison of the pitch altitude in carrier air-wake.

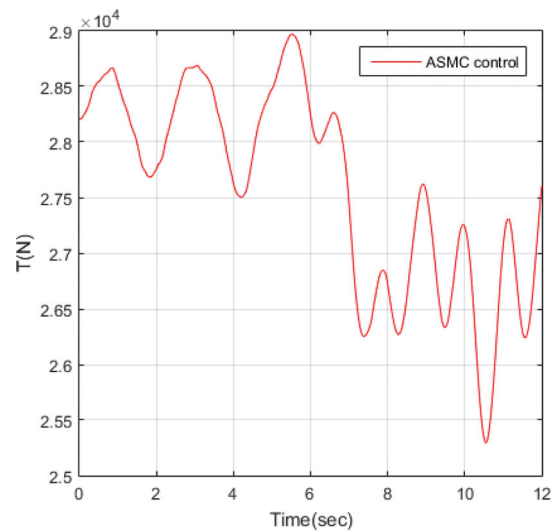


Figure 14 Comparison of the thrust in carrier air-wake.

By analyzing the trend of the curve in the final-approach as shown in Figures 8–16, it can be seen that due to the influence of the carrier air-wake, the performance of the system is changing and the suppression ability of APCS based on ASMC is better than the normal APCS.

## 6. CONCLUSION

By analyzing the signal flow chart of the ACLS, we obtained the velocity change relation of carrier-based aircraft and the speed stability criterion to determine the necessity of the APCS. It has been proven that the speed of carrier-based aircraft is unstable during the carrier landing task when the aerodynamic parameters and derivative are brought to the criterion. Hence, the APCS is necessary for the ACLS.

In the final-approach, this paper has established the six-degree of freedom non-linear model of the carrier-based aircraft and the model of carrier air-wake. A comparison of the capability to suppress the carrier air-wake with the normal design of the APCS and the APCS based on ASMC, shows that the anti-interference ability of the APCS based on the ASMC is better than the normal APCS, and the tracking ability of glide slope based on the ASMC is improved. The simulation result shows that in the final-approach, the APCS based on the ASMC keeps the AOA constant better than does the normal design. The anti-interference ability to carrier air-wake is obviously enhanced and the chattering phenomenon is effectively reduced.

## 7. ACKNOWLEDGEMENTS

This study was co-supported by the National Natural Science Foundation (NNSF) of China under Grant 61603110 and the National Natural Science Foundation (NNSF) of China under Grant 61803116. International Science & Technology Cooperation Program of China under Grant 2013DFR10030 and fundamental research funds for the central universities under Grant HEUCFM170401.

## REFERENCES

1. Peng Jing. Research on the automatic guide and control of a carrier-based airplane approach and landing[D]. Beijing: Beihang University, 2001: 167–170.
2. Guihua Xia, Ran Dong. Linearized Model of Carrier-Based Aircraft Dynamics in Final-Approach Air Condition[J]. *Journal of Aircraft*, 2015, 53(1): 1–15.
3. Wang X H, Yang Yidong, Zhu Hua. Study on the control characteristics of the aircraft under the condition of low dynamic pressure [J]. *Flight Dynamics*, 2007, 25(4): 29–32.
4. Li X, Wu W H. Study on flight control characteristics of carrier aircraft landing aircraft [J]. *Flight Dynamics*,
5. Liu S L. Research on automatic Power compensation of carrier aircraft [D]. Shenyang: Dongbei University, 2011:15–17.
6. Yu Yongtao. Research on Crucial Technology of Automatic Carrier Landing System[D]. Harbin: Harbin Engineering University, 2010.
7. Deng Juan. Theory and simulation for the design of longitudinal automatic carrier landing system[D]. Shanghai: Fudan University, 2010:30–5.
8. Xia Guihua, DONG Ran, MENG Xue, et al. Research on the dynamic modeling for the landing of a carrier-based aircraft[J]. *Journal of Harbin Engineering University*, 2014, 35(4): 445–456.
9. Wang W J, MA H Z, LIU C L. Integrated flight/vectored thrust control for UAV[J]. *Acta Aeronautica et Astronautica Sinica*, 2008(S1):150–156.
10. Zhu Q D, Yu Y T, Zhang W. Discrete variable structure control design for APCS of carrier-based aircraft based on dynamic disturbance compensation[C]// *IEEE, International Conference on Industrial Engineering and Engineering Management*. IEEE, 2011:1671–1675.
11. Man Cuifang, Jiang Ju, Wang Xinhua, et al. Carrier-Based Aircraft Approach Power Compensator System Design Based on Fuzzy Logic Techniques[J]. *JOURNAL OF NANJING UNIVERSITY OF AERONAUTICS & ASTRONAUTICS*, 2010, 42(05):656–660.
12. Chen Jun-feng<sup>1</sup>, Han Wei<sup>1</sup>, Hu Yang. Power compensation system simulation of carrier-based aircraft landing with high-order sliding mode[J]. *Flight Dynamics*, 2015, 33(01):26–29.
13. Yu Yong, Yang Yidong, Dai Shijun. Study of Flight/Thrust Control System Using  $H_{\infty}$  Synthesis in Carrier Landing System[J]. *Journal of Nanjing University of Science and Technology*, 2003(03):256–260.

14. Anderson M. Inner and outer loop manual control of carrier aircraft landing[C]// Guidance, Navigation, and Control Conference. 2015: 71–92.
15. Joseph M, Sweger F. Design Specifications Development for Unmanned Aircraft Carrier Landings: A Simulation Approach[J]. 2003.
16. AIAA. An Autonomous Carrier Landing System for Unmanned Aerial Vehicles - AIAA Guidance, Navigation, and Control Conference (AIAA)[J]. AIAAJournal, 2009.
17. Zhu Qi-dan, Meng Xu. Fault tolerant control for longitudinal carrier landing system with application to aircraft [J]. Control Theory & Applications,2017,34(10):1311–1320.
18. Zhang Zhi, Li Jiatong, Dong Ran, et al. Optimal design of longitudinal automatic carrier landing system for carrier air wake rejection[J], Journal of Harbin Engineering University, 2016,37(06):802–811.
19. Liu Jin-kun. The Matlab Simulation of Sliding Mode Variable Structure Control [M]. Beijing: Tsinghua University Press, 2005.
20. Slotine, J.-J. E. (Jean-Jacques E.), Li, Weiping. Applied nonlinear control[M]. China Machine Press, 2004:21–90.